J. Iron Steel Res. Int.
https://doi.org/10.1007/s42243-018-0047-x

ORIGINAL PAPER

Impacts of multiple laser shock processing on microstructure and mechanical property of high-carbon steel

Yi Xiong[1,2] · Tian-tian He[1] · Yan Lu[1] · Han-sheng Bao[3] · Yong Li[3] · Feng-zhang Ren[1,2] · Wei Cao[4,5] · Alex A. Volinsky[6]

Received: 17 April 2017 / Revised: 25 June 2017 / Accepted: 3 July 2017

Abstract
Multiple laser shock processing (LSP) impacts on microstructures and mechanical properties were investigated through morphological determinations and hardness testing. Microscopic results show that without equal channel angular pressing (ECAP), the LSP-treated lamellar pearlite was transferred to irregular ferrite matrix and incompletely broken cementite particles. With ECAP, LSP leads to refinements of the equiaxed ferrite grain in ultrafine-grained microduplex structure from 400 to 150 nm, and the completely spheroidized cementite particles from 150 to 100 nm. Consequentially, enhancements of mechanical properties were found in strength, microhardness and elongations of samples consisting of lamellar pearlite and ultrafine-grained microduplex structure. After LSP, a mixture of quasi-cleavage and ductile fracture was formed, different from the typical quasi-cleavage fracture from the original lamellar pearlite and the ductile fracture of the microduplex structure.

Keywords Laser shock processing · High-carbon steel · Ultrafine-grained microduplex structure · Mechanical property

1 Introduction

As a surface modification technique, the laser shock processing (LSP) is advanced in super-high strain rate deformation of the metal surface thanks to the intensive pulsed laser-induced plasma wave detonations [1]. The peak stress of the laser-induced shock wave is greater than material dynamic yield strength. Consequently, plastic deformation occurs on the metal surface with intensive stable dislocation structure, while residual compressive stress in hundreds of MPa level is produced simultaneously in the metal surface layer. LSP can effectively improve strength [2], abrasive [3] and corrosion resistance [4], along with the fatigue life [5] of materials. To date, LSP has been widely used in advanced manufacturing. For instance, LSP has been employed in surface treatments for titanium alloys [6], magnesium alloys [7], aluminum alloys [8], coppers alloys [9], austenitic stainless steels [10], carbon steels [11], etc. Despite these progresses, only microstructure response and property change in the single-phased materials have been revealed under LSP super-high strain rate deformation. Though microstructure evolution and mechanical properties of microduplex structure were revealed during LSP [12, 13], structural evolutions and property modifications with different structural states remain unclear.

Understanding microstructure evolution and relevant property variations in different original metal structures processed under the same deformation conditions allows establishing relations between microstructure response and strain-hardening effects. As a result, it could provide basis

✉ Yi Xiong
xy_hbdy@163.com

1 School of Materials Science and Engineering, Henan University of Science and Technology, Luoyang 471023, Henan, China

2 Collaborative Innovation Center of Nonferrous Metals, Luoyang 471023, Henan, China

3 Institute for Special Steels, Central Iron and Steel Research Institute, Beijing 100081, China

4 Nano and Molecular Systems Research Unit, University of Oulu, 90014 Oulu, Finland

5 School of Mechanical and Automotive Engineering, Anhui Polytechnic University, Wuhu 241000, Anhui, China

6 Department of Mechanical Engineering, University of South Florida, Tampa, FL 33620, USA

Published online: 05 April 2018

for developing further processing techniques and reasonable materials selection. For these reasons, impacts of LSP on microstructure evolution and mechanical properties of high-carbon steel with two different original structures of lamellar pearlite and ultrafine-grained microduplex structure were investigated in the present study. It is hoped that this work can provide insightful experimental supports for the development and applications of LSP on high-carbon steel.

2 Materials and experimental procedure

The investigated steel ingot was manufactured from Fe–0.8C steel with the following chemical composition (in wt%): C 0.82, Mn 0.33, Si 0.24, P 0.011, S 0.012 and Fe balance. Samples were austenitized at 1273 K for 30 min and then were treated at 873 K for 30 min in a salt bath furnace to obtain the original structure with lamellar pearlite. Ultrafine-grained microduplex structures were prepared by subsequent equal channel angular pressing (ECAP).

The samples used for ECAP were cut into cylinders with dimensions of 8.3 mm in diameter and 49 mm in length. The intersecting angle between the two channels was 120°, and the angle of the outer arc at the intersection was 30°. The four-pass ECAP processing was performed at 923 K using the Bc route method. These ECAP specimens were rotated by 90° along the longitudinal axis of the specimen after each pass in order to obtain a homogeneous microstructure. Before put in the entrance channel at the testing temperature, the specimen and the die were both coated with graphite and MoS_2 for lubrication. The detailed processing procedure can be found in the previous work [14]. Mini-tensile test specimens of lamellar pearlite and ultrafine-grained microduplex structure were sectioned along the longitudinal axis by wire cutting, as shown in Fig. 1a. Then, the sample surface was polished and cleaned in deionized water. Subsequent LSP treatment was conducted on the gauge surface of the sample.

The LSP experiments were performed using a solid-state Nd:glass phosphate laser with a wave length of 1.064 μm and a pulse duration of about 10 ns. Water layer with thickness of 1 mm was used as the transparent confining layer, while 100-μm-thick aluminum tape was used as the absorbing layer. The spot diameter was 3 mm, the LSP impact time was 4 times, the laser energy was 6 J, and the overlapping was 50% [15]. The parameters used in LSP are shown in Table 1.

Microstructure characterization was carried out using field emission scanning electron microscopy (SEM) and transmission electron microscopy (TEM). For metallographic examination, samples were prepared by electrolytic etching using 4% nital solution after LSP. For TEM observation, disks mechanically thinned to 40 μm were prepared using ion polishing system. Operating voltage of TEM was set to 200 kV.

The mini-tensile test was conducted on the Instron 5948R micromaterial testing machine with a chuck moving velocity of 0.1 mm/min. The morphology of the fracture surfaces was observed using scanning electron microscopy, operated at 20 kV. Subsequently, microhardness of the laser processed regions was measured by using HV-1000A Vickers microhardness tester. The load was 2 N, and the holding time was 10 s. The laser processed regions with the interval distance of 0.2 mm along the longitudinal axis, as shown in Fig. 1b.

3 Results and discussion

3.1 Microstructure evolution of high-carbon steel before LSP

Figure 2 shows the SEM and TEM images of the high-carbon steel with different original structures before LSP treatment. In Fig. 2a, Fe–0.8C steel shows full lamellar pearlitic structure after isothermal treatment at 600 °C.

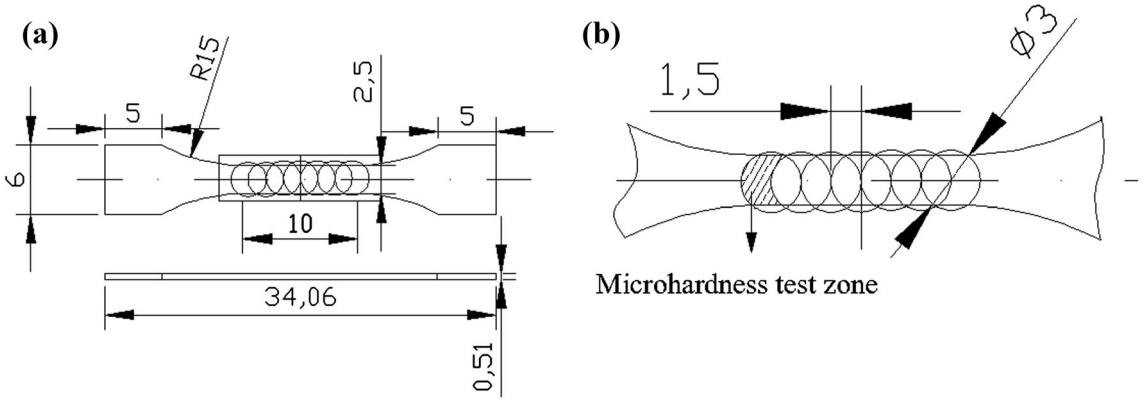

Fig. 1 Dimensions of mini-tensile sample. **a** Dimensions of tensile sample; **b** partially enlarged drawing of treated area subjected to LSP (unit: mm)

Table 1 Processing parameters used in LSP

Type	Value
Beam divergence of output/mrad	≤ 2
Spot diameter/mm	3
Pulse energy/J	6
Impact times	4
Pulse width/ns	10
Repetition rate/Hz	5
Laser wavelength/nm	1064
Pulse to pulse energy stability/(% rms)	< 1.5

After four ECAP passes, the original pearlitic lamellae disappeared totally, but traces of arrangement direction of the initial cementite lamellae can be observed. To accommodate the shear deformation of ECAP, the cementite lamella are severely bent and kinked. Meanwhile, spheroidization of the cementite occurred and increased with deformation, as observed in Fig. 2b. From TEM micrographs in Fig. 2c, d, the lamellae spacing of the cementite is determined to ∼ 150 nm, and thickness is to ∼ 30 nm (Fig. 2c). Figure 2d shows the ultrafine-grained microduplex structure with submicron grain size after four ECAP passes. The sizes of equiaxed ferrite grains and the cementite particles are about 400 and 150 nm, respectively. During the warm deformation, the equiaxial process of ferrite coordinates with the spheroidization of the cementite lamellae [16]. During the initial stage of plastic deformation, high-density dislocation lines develop in the ferrite grains. The dislocation tangles and dense dislocation cells are formed due to pileup of the dislocation lines [17, 18]. Some sub-grains of the dislocated cells become sharper as strain increases. Then, high-angle grain boundaries develop due to the continuous dynamic recrystallization in the sub-grain boundaries, which refines the

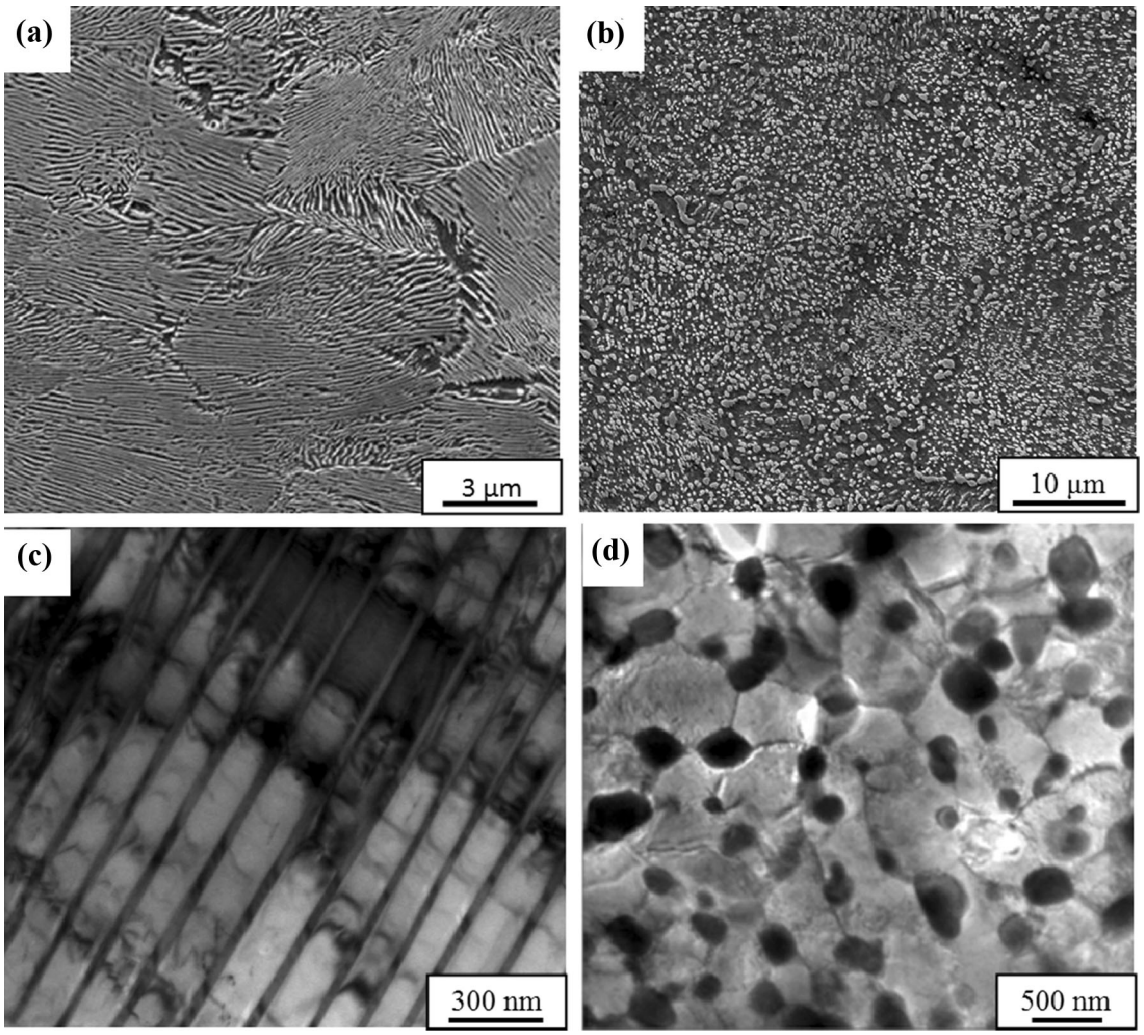

Fig. 2 Micrographs of the high-carbon steel before LSP. **a** SEM morphology of lamellar pearlite; **b** SEM morphology of ultrafine-grained microduplex structure; **c** TEM morphology of lamellar pearlite; **d** TEM morphology of ultrafine-grained microduplex structure

ferrite grains [15, 19]. Meanwhile, the diffusion of Fe and C atoms is speeded up due to the dislocation tangles and sub-grain boundaries, accelerating cementite spheroidization process.

3.2 Microstructure evolution of high-carbon steel after LSP

Figure 3 shows microscopic images of the high-carbon steel with two different original microstructures after LSP. SEM figures (Fig. 3a, b) show that the lamellar pearlitic structure is kinked, bent and fractured at the same time along with the breaking of the cementite lamellae. However, the orientation is still kept in Fig. 3a. After multiple LSP treatments, the cementite of ultrafine-grained microduplex structure is completely fractured into granules, and particle diameter decreases from 150 to 100 nm (Fig. 3b). As indicated by the corresponding TEM micrographs shown in Fig. 3c, d, after LSP of the lamellar pearlitic structure, more dislocations are formed and dislocation density obviously increases in the ferrite matrix. The parallel lamellar pearlites are broken into some segments, and dislocation activities simultaneously lead to the formation of dislocation lines and dislocation tangles in the ferrite grains. With increasing number of laser shocks, the broken lamellar pearlites are further fragmented to bitty pearlites. These dislocation configurations gradually developed to subdivision of ferrite grains by forming individual primarily separated dislocation cells. Consequently, the ferrite matrix was refined and represented by $\sim$ 700 nm irregular ferrite grains. However, the cementite lamellae are insufficiently broken into bitty cementite; most of them are on the grain boundaries, and a few completely broken cementite particles are located in the ferrite grains (Fig. 3c). In contrast, after LSP treatment for the ultrafine-grained microduplex structure, as shown in Fig. 3d, the ferrite grain is further refined and the fragmentation of cementite granules is more complete. The average grain size of equiaxed ferrite grains and completely fractured cementite particles are further refined to about 150 and 100 nm, respectively (Fig. 3d). This is in accordance with the observation in Ref. [20], where grains in the surface layer of ANSI 304 stainless steel subjected to multiple LSP impacts were extremely refined down to $\sim$ 50–200 nm at the top surface. Besides, Lemiale et al. [21] studied the grain size change in the ultrafine-grained materials after high strain rate deformation by using the finite elements software based on dislocation viscoplastic model. Therein, the grain size of the ultrafine grain materials can be further refined under high strain rate deformation. Results in the present study agree well with these previously reported findings.

3.3 Mechanical properties and microhardness of high-carbon steel after LSP

The engineering stress–strain curves from the mini-tensile test of the high-carbon steel with different original structures before and after LSP are shown in Fig. 4. The LSP enhances strength and elongation of the high-carbon steel with different original structures. The ultimate tensile strengths increase from (867 ± 5) (lamellar pearlite structure) and (819 ± 5) MPa (ultrafine-grained microduplex structure) to (920 ± 5) and (871 ± 5) MPa, respectively. The corresponding yield strengths increase from (477 ± 5) and (662 ± 5) MPa to (520 ± 5) and (685 ± 5) MPa, respectively. Meanwhile, after LSP, the elongation significantly increased from 5 and 18% to 10 and 20% for the lamellar pearlite structure and ultrafine-grained structure, respectively. The local plastic deformation after LSP leads to the generation of the compressive residual stresses near the specimen surface. Indeed, here the high-intensity short-pulsed laser beam bombards and vaporizes opaque sacrificial coating on the metal workpiece. Vapor and plasma absorb the incident laser energy and violently explode against the metal surface. A portion of the energy propagates as a shock wave into the metal. When the shock wave pressure exceeds metal yield strength, metal deforms plastically and a large amount of dislocations occur. Thus, a layer with residual compressive stress forms on its surface [22]. The fatigue performance can be improved by the compressive residual stress, which can inhibit the fatigue crack initiation and growth, and prolong the crack propagation life [23]. Consequentially, after LSP, mechanical properties of the high-carbon steel with different original structures are enhanced by the compressive stress at the surface.

Microhardness of the high-carbon steel with different original structures after LSP is shown in Fig. 5. Surface hardness obviously increases after LSP for the samples with two different original structures. Increase in the hardness at the center of the laser spot is much higher than regions farther apart from the spot. This is because the stress induced by the shock wave has a Gaussian distribution due to the intrinsic character of the laser pulse energy. The microhardness of ultrafine-grained microduplex structure is increased by 27% from 296 to 376 HV at the impact center. The percentage is about 2 times of the increase in initial lamellar pearlite structure, i.e., by 14% from 302 to 342 HV. After LSP of the lamellar pearlitic structure, there is severe plastic deformation in the metal surface, resulting in the increase in the dislocation density, formation of dislocation cells and pinning of dislocations. Meanwhile, large stress concentration emerged in the local area, leading to obvious work hardening. Furthermore, the

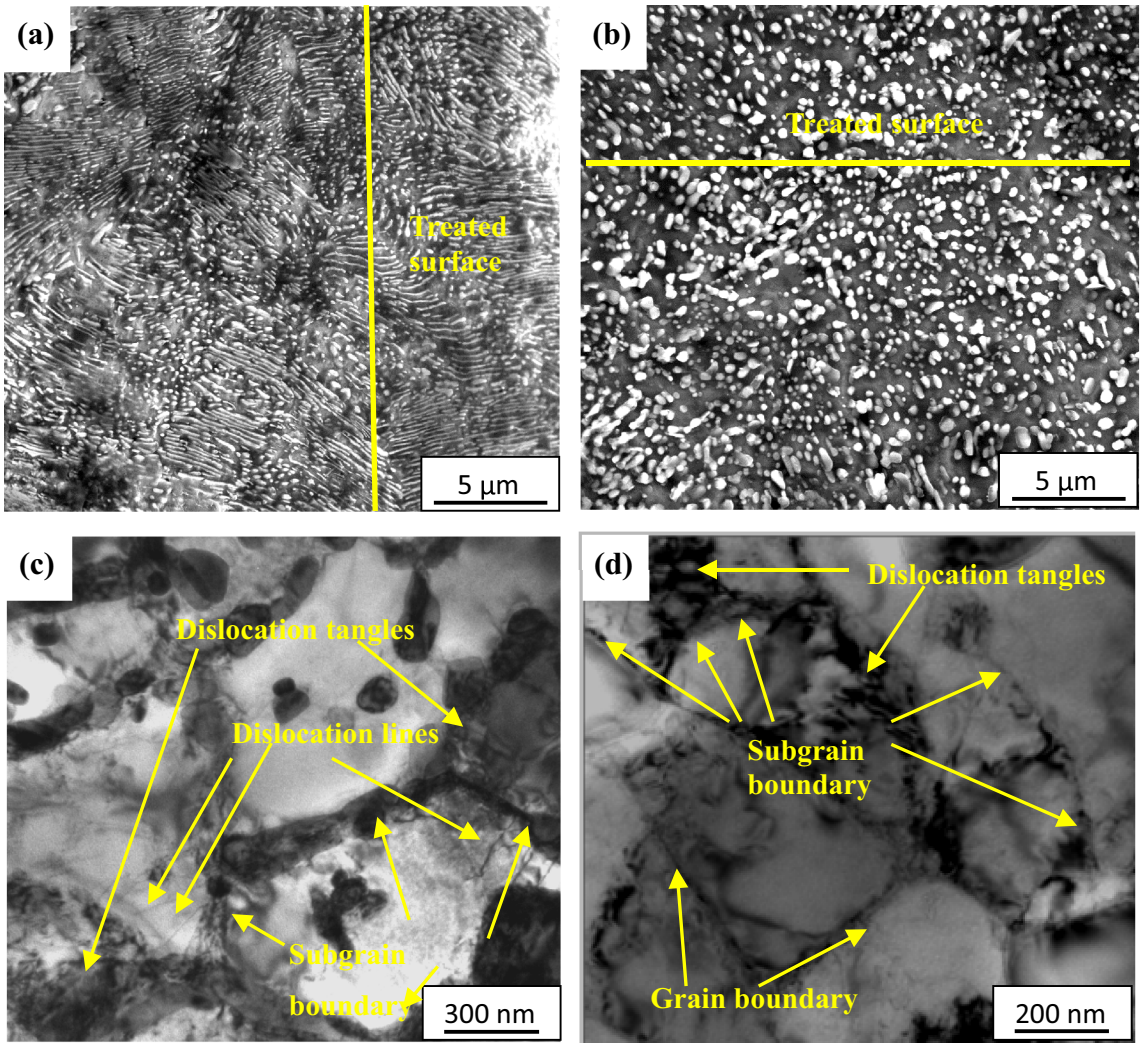

Fig. 3 Micrographs of the high-carbon steel after LSP. **a** SEM morphology of lamellar pearlite; **b** SEM morphology of ultrafine-grained microduplex structure; **c** TEM morphology of lamellar pearlite; **d** TEM morphology of ultrafine-grained microduplex structure

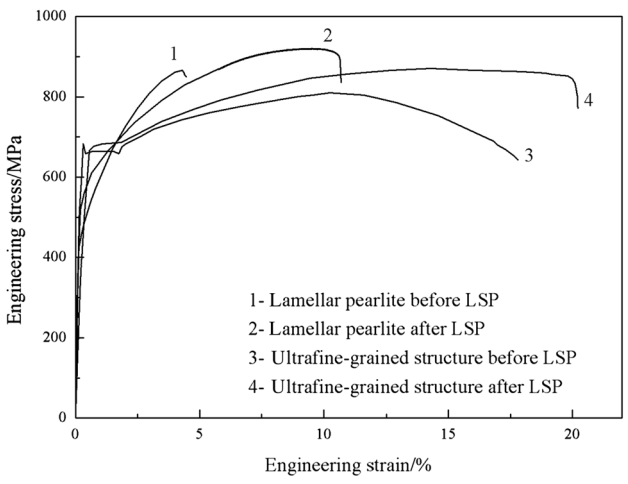

Fig. 4 Engineering stress–strain curves from mini-tensile test of high-carbon steel with different original structures before and after LSP

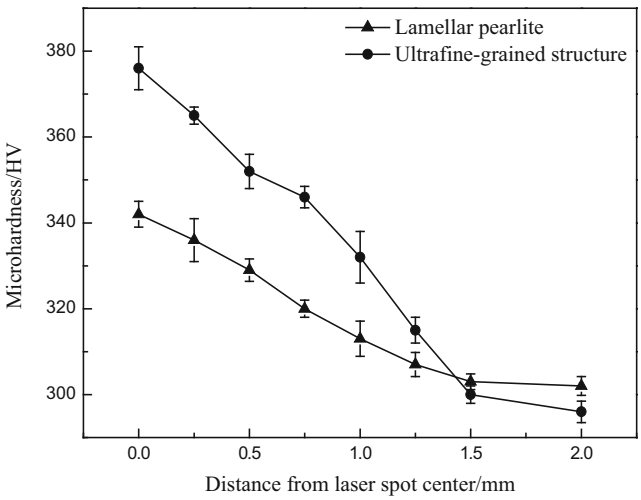

Fig. 5 Microhardness of high-carbon steel with different original structures after LSP

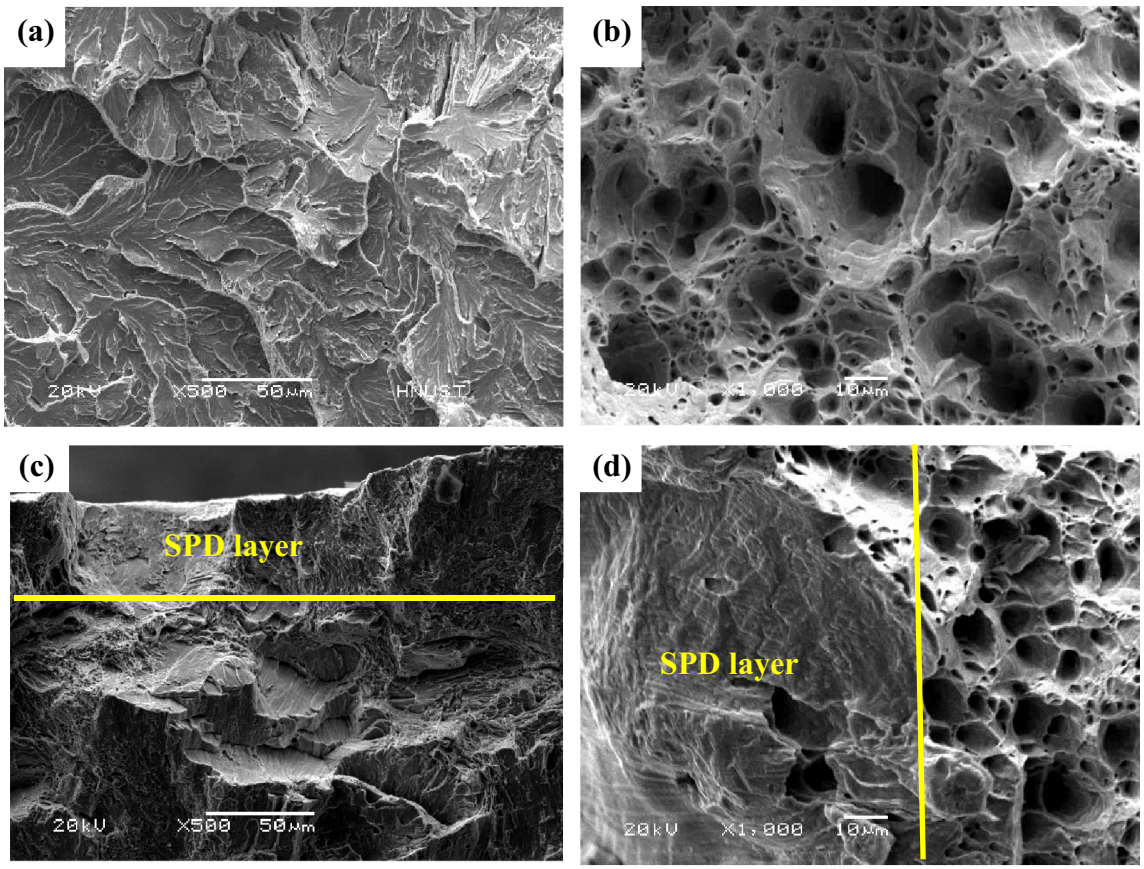

Fig. 6 Fracture surface morphology of high-carbon steel with two different initial microstructures before and after LSP. **a** Before LSP of lamellar pearlite; **b** before LSP of ultrafine-grained microduplex structure; **c** after LSP of lamellar pearlite; **d** after LSP of ultrafine-grained microduplex structure

ferrite grain is refined to 700 nm (Fig. 3c). As a result, the hardness is evidently improved. At the same time, the cementite lamellae are kinked, bent, fractured and broken into granules constantly in the lamellar pearlite structure, decreasing microhardness. The microhardness at the center of the laser spot of the lamellar pearlite increases slowly under the combined interactions of work hardening, grain refinement and the fragmentation of cementite. After LSP of the ultrafine-grained microduplex structure, the ferrite is further refined (Fig. 3d). The fragmentation of cementite granules is more complete, and their size is further decreased. Meanwhile, partial dissolution of the cementite occurs, leading to supersaturated carbon atoms. This phenomenon was proved by the previous work [24]. Microhardness in the impact center of ultrafine-grained microduplex structure increases remarkably, compared to that of lamellar pearlite structure. This is mainly due to grain refinement and solution strengthening. However, the hardness and the ultimate tensile strength do not follow the basic law where hardness is one-third of the ultimate tensile strength. This is mainly because after LSP, a gradient structure was formed from the sample surface to the core [20]. Thus, the ultimate tensile strength represents the overall performance of the samples, while the hardness is tested at the sample surface.

3.4 Fracture surface morphology

The fracture surface morphology of the high-carbon steel with two different original microstructures before and after LSP is shown in Fig. 6. Before LSP, the fracture surfaces of the original lamellar pearlite structure and ultrafine-grained microduplex structure are quasi-cleavage fracture and ductile fracture, respectively. In Fig. 6a, a typical river-like pattern can be observed and a small amount of microcracks and tear ridges exist around the river pattern. The fracture surface of the sample is smooth and decorated with dimples varying in sizes and depths. The average size of a few large and deep dimples is about 8 μm, while a large number of small and shallow dimples are distributed uniformly at an average size of ~ 1 μm (see Fig. 6b). After LSP, the fracture morphology shows a mixture of quasi-cleavage and ductile fracture. The quasi-cleavage fracture occurs both at the sample surface (ultrafine-

grained microduplex structure) and inside the sample (lamellar pearlite structure), while ductile fractures exist inside the sample (ultrafine-grained microduplex structure) and at the sample surface (lamellar pearlite structure). This is mainly due to the severe plastic deformation (SPD) layer with a certain depth (about 50 μm) at the sample surface after LSP, as shown in Fig. 6c, d. For the lamellar pearlite structure, cementite lamellar fracture in the plastic deformation layer improves the plastic deformation capacity of the lamellar pearlite structure. The fracture surface shows ductile fracture. For the ultrafine-grained microduplex structure, work hardening occurs in the plastic deformation layer, which results in the quasi-cleavage fracture. Thus, the fracture surface of the two different original microstructures of the high-carbon steel after LSP is a mixture of quasi-cleavage and ductile fracture. This is consistent with the results of LY2 alloy after multiple LSP by Lu et al. [25]. Figure 6 shows that the gradient structure forms in the high-carbon steel after LSP. With the increase in the distance to the treated surface, the microstructure evolves from dislocation lines (inside the sample) to dislocation tangles and dislocation walls (subsurface), and to sub-grains and ultrafine grains (outer surface). This may be attributed to decreases in the strain and stress following the increase in distance to the treated surface [15].

4 Conclusions

1. The microstructure of high-carbon steel with different original structures was effectively refined by multiple LSP. The lamellar pearlite changed into irregular ferrite matrix and incompletely broken cementite particle after LSP. The ferrite grain size is 700 nm. Equiaxed ferrite grains and completely spheroidized cementite particles in ultrafine-grained microduplex structure were further refined from 400 and 150 nm to about 150 and 100 nm grain size, respectively.
2. Mechanical properties of the high-carbon steel with different original microstructures are improved after multiple LSP. The microhardness of ultrafine-grained microduplex structure increased 27%, which is 2 times higher than that of the initial lamellar pearlite structure of 14%. Meanwhile, after LSP, the elongation of the lamellar pearlite sharply increased.
3. The fracture surface morphology changes from typical quasi-cleavage fracture (lamellar pearlite) and ductile fracture (ultrafine-grained microduplex structure) to a mixture of quasi-cleavage and ductile fracture after LSP.

Acknowledgements This work was supported by the NSFC (50801021, 51201061) and by Program for Science, Technology Innovation Talents in Universities of the Henan Province (17HASTIT026), the Science and Technology Project of the Henan Province (152102210077), International Scientific and Technological Cooperation Project from Science and Technology Department of Henan Province (172102410032), Education Department of the Henan Province (16A430005) and the Science and Technology Innovation Team of the Henan University of Science and Technology (2015XTD006).

References

[1] C.S. Montross, T. Wei, L. Ye, G. Clark, Y.W. Mai, Int. J. Fatigue 24 (2002) 1021–1036.
[2] B.P. Fairand, B.A. Wilcox, W.J. Gallagher, D.N. Williams, J. Appl. Phys. 43 (1972) 3893–3895.
[3] J.Z. Lu, K.Y. Luo, F.Z. Dai, J.W. Zhong, L.Z. Xu, C.J. Yang, L. Zhang, Q.W. Wang, J.S. Zhong, D.K. Yang, Y.K. Zhang, Mater. Sci. Eng. A 536 (2012) 57–63.
[4] H. Lim, P. Kim, H. Jeong, S. Jeong, J. Mater. Process. Technol. 212 (2012) 1347–1354.
[5] X.F. Nie, W.F. He, S.L. Zang, X.D. Wang, J. Zhao, Surf. Coat. Technol. 253 (2014) 68–75.
[6] J.Z. Lu, L.J. Wu, G.F. Sun, K.Y. Luo, Y.K. Zhang, J. Cai, C.Y. Cui, X.M. Luo, Acta Mater. 127 (2017) 252–266.
[7] M.Z. Ge, J.Y. Xiang, J. Alloy. Compd. 680 (2016) 544–552.
[8] S. Huang, J.Z. Zhou, J. Sheng, K.Y. Luo, J.Z. Lu, Z.C. Xu, X.K. Meng, L. Dai, L.D. Zuo, H.Y. Ruan, H.S. Chen, Int. J. Fatigue 47 (2013) 292–299.
[9] J. Cai, S. Shekhar, J. Wang, M.R. Shankar, Scripta Mater. 60 (2009) 599–602.
[10] J.Z. Lu, J.S. Zhong, K.Y. Luo, L. Zhang, H. Qi, M. Luo, X.J. Xu, J.Z. Zhou, Surf. Coat. Technol. 221 (2013) 88–93.
[11] C. Ye, S. Suslov, B.J. Kim, E.A. Stach, G.J. Cheng, Acta Mater. 59 (2011) 1014–1025.
[12] C.R. González, C.F. Martinez, G.G. Rosas, J.L. Ocâna, M. Morales, J.A. Porro, Mater. Sci. Eng. A 528 (2011) 914–919.
[13] X.M. Luo, G.Z. Zhao, Y.K. Zhang, K.M. Chen, K.Y. Luo, X.D. Ren, Acta Metall. Sin. 48 (2012) 1116–1122.
[14] T.T. He, Y. Xiong, F.Z. Ren, Z.Q. Guo, A.A. Volinsky, Mater. Sci. Eng. A 535 (2012) 306–310.
[15] J.Z. Lu, K.Y. Luo, Y.K. Zhang, C.Y. Cui, G.F. Sun, J.Z. Zhou, L. Zhang, J. You, K.M. Chen, J.W. Zhong, Acta Mater. 58 (2010) 3984–3994.
[16] E. Werner, Acta Mater. 37 (1989) 2047–2053.
[17] R. Kaspar, W. Kapellner, C. Lang, Steel Res. Int. 59 (1988) 492–498.
[18] E.A. Chojnowski, W.J.M. Tegart, Metal Sci. J. 2 (1968) 14–18.
[19] J.Z. Lu, J.W. Zhong, K.Y. Luo, L. Zhang, F.Z. Dai, K.M. Chen, Q.W. Wang, J.S. Zhong, Y.K. Zhang, Mater. Sci. Eng. A 528 (2011) 6128–6133.
[20] J.Z. Lu, K.Y. Luo, Y.K. Zhang, G.F. Sun, Y.Y. Gu, J.Z. Zhou, X.D. Ren, X.C. Zhang, L.F. Zhang, K.M. Chen, C.Y. Cui, Y.F. Jiang, A.X. Feng, L. Zhang, Acta Mater. 58 (2010) 5354–5362.
[21] V. Lemiale, Y. Estrin, H.S. Kim, R.O. Donnell, Comput. Mater. Sci. 48 (2010) 124–132.
[22] Z. Zhou, S. Bhamare, G. Ramakrishnan, S.R. Mannava, K. Langer, Y.H. Wen, D. Qian, V.K. Vasudevan, Surf. Coat. Technol. 206 (2012) 4619–4627.
[23] X.D. Ren, Q.B. Zhan, H.M. Yang, F.Z. Dai, C.Y. Cui, G.F. Sun, L. Ruan, Mater. Des. 44 (2013) 149–154.
[24] Y. Xiong, T.T. He, F.Z. Ren, P.Y. Li, L.F. Chen, A. A.Volinsky, J. Iron Steel Res. Int. 22 (2015) 55–59.
[25] J.Z. Lu, K.Y. Luo, Y.K. Zhang, J.Z. Zhou, X.G. Cui, L. Zhang, J.W. Zhong, Mater. Sci. Eng. A 528 (2010) 730–735.